UNCLASSIFIED

Defense Technical Information Center
Compilation Part Notice

ADP014254

TITLE: Effect of Solid-Solution W Addition on the Nanostructure of Electrodeposited Ni

DISTRIBUTION: Approved for public release, distribution unlimited

This paper is part of the following report:

TITLE: Materials Research Society Symposium Proceedings Volume 740 Held in Boston, Massachusetts on December 2-6, 2002. Nanomaterials for Structural Applications

To order the complete compilation report, use: ADA417952

The component part is provided here to allow users access to individually authored sections of proceedings, annals, symposia, etc. However, the component should be considered within the context of the overall compilation report and not as a stand-alone technical report.

The following component part numbers comprise the compilation report:
ADP014237 thru ADP014305

UNCLASSIFIED

Mat. Res. Soc. Symp. Proc. Vol. 740 © 2003 Materials Research Society I3.28

Effect of Solid-Solution W Addition on the Nanostructure of Electrodeposited Ni

Hajime Iwasaki, Kenji Higashi[1] and T. G. Nieh[2]

Department of Materials Science & Engineering, Himeji Institute of Technology
2167 Shosha, Himeji, Hyogo 671-2201, Japan
[1] Department of Metallurgy and Materials Science, College of Engineering, Osaka Prefecture University, Sakai 599-8531, Japan
[2] Lawrence Livermore National Laboratory, L-350, PO Box 808, Livermore, CA 94551, USA

ABSTRACT

Electrodeposition method was employed to produce freestanding Ni-W alloy foils. The foils consist of nanograins. The structure of the foil, e.g. texture, grain morphology, size distribution, and the nature of grain boundaries, were characterized using X-ray diffraction and high-resolution electron microscopy. The deposited foils exhibit an equiaxed nanocrystalline structure having a grain size value of about 6 nm. Two types of grain boundary structure were observed. One type of grain boundary is essentially one atomic layer thin and another type consists of a structureless layer of about 0.5-1 nm in thickness. Angular dark field (Z-contrast) image of the deposited foils showed an inhomogeneous distribution of W solutes. In some local regions, the W content actually exceeds the equilibrium solid solution limit. Many grain boundaries with a structureless layer of about 0.5-1 nm are probably a result of local supersaturation of W.

INTRODUCTION

The technological development of nanocrystalline alloys has been driven by the promise of exceptional properties. Scientifically, the study of nanocrystalline materials is also of great interest because the potential breakdown of classical scaling laws and the accompanying need for new materials physics in the nanostructured limit. However, materials with grain sizes below about 10 nm are still extremely difficult to produce. Electrodeposition is a viable method to produce fine-structured material. However, to produce nanocrystalline materials using electrodeposition, fine grain sizes apparently require a compromise in purity. For example, the addition of a nucleation agent during electrodeposition can reduce the grain size of the nanocrystalline product, but it also increases the carbon and sulfur content of the alloy [1,2]. Alternatively, finer grain sizes can be achieved via alloying, as demonstrated in Fe-Ni [3,4] and other systems [5,6]. Alloying has long been recognized as an effective method to increase glass-forming ability and, in fact, is critical for the production of bulk amorphous metals and devitrified nanocrystalline alloys [7]. Considered collectively, the above studies suggest that fine-structured nanocrystalline metals (from amorphous to ~10 nm grain size) are achievable through the use of a low-temperature single-step production process and a careful selection of alloy composition.

In the present work, we study the grain and grain boundary structures of nanocrystalline Ni-W alloys with grain sizes below 10 nm produced by direct current (DC) electrodeposition. Prior research has shown that Ni-W alloys can be refined to a fully amorphous structure by judicious design of the plating bath [8]. Thereby, this system offers the potential to observe the transition in mechanical properties from the nanocrystalline to the amorphous state. Additionally, Ni-W alloys have been targeted for the application of micro-fabrication technologies, where their improved hardness and abrasion resistance are attractive [9].

EXPERIMENTAL DETAILS

Electrodeposition of Ni-W alloys has been discussed at length previously [8,9]. Here we have used a similar method to produce foils about 20 μm thick; the composition of the plating bath is given in Table I. Citric acid and ammonium chloride were introduced to form complexes with Ni and W, while sodium bromide was used to improve conductivity. An electro-polished copper sheet of 25 x 30 x 1 mm was used as the plating substrate, and the anode was high purity platinum. A 500 mL bath was maintained at 72° C, and the applied DC current density was constant at 0.05, 0.10 or 0.15A/cm^2. A new plating bath was made of analytical reagent-grade chemicals and pure water for each experiment.

After plating, the Cu substrate was dissolved in an aqueous solution containing 250 g/L of CrO_3 and 15 cm^3/L H_2SO_4. All electrodeposited foils were degassed in vacuum at 80°C for 24 h. Chemical analysis of the electrodeposited alloys was carried out by means of spectroscopic analysis in an inductively coupled argon-plasma (to determine metal content), and for one foil the oxygen and hydrogen content were assessed by measuring the amount H_2O formed after melting the alloy. Structural analysis was also performed by means of X-ray diffraction (XRD) using Cu-Kα radiation in a Rigaku RINT –1500 operating at 40 kV and 200 mA.

Microstructural observations were performed using high-resolution electron microscopy (HREM) on the normal plane of the electrodeposited foils. The high-resolution transmission electron microscopy is JEM-4000EX, operated at 400 kV.

DISCUSSION

Table I: Composition of the plating bath for Ni-W electrodeposition.

Nickel Sulfate ($NiSO_4$-$6H_2O$)	0.06 mol/L
Citric Acid ($Na_3C_6H_5O_7$-$2H_2O$)	0.5 mol/L
Sodium Tungstate (Na_2WO_4-$2H_2O$)	0.14 mol/L
Ammonium Chloride (NH_4Cl)	0.5 mol/L
Sodium Bromide (NaBr)	0.15 mol/L

Table II: Chemical and physical properties of Ni-W electrodeposits.

Current Density (A/cm^2)	W content (at%)	XRD grain Size (nm)	TEM grain Size (nm)	Texture (<110> ‖ thickness)
0.05	11.6	7	~5	Strong
0.10	11.8	-	4.5-6.2	Moderate
0.15	12.4	-	~4	Near Random

Composition and nano-structure

The chemical and physical properties of the electrodeposited Ni-W films, as well as the current density used to produce the films, are listed in Table II. All of the alloys exhibited a W content in the narrow range of 12.0 ± 0.4 at%, slightly increases with an increasing applied current density. Analysis from the specimen synthesized at a current density of 0.10 A/cm^2 indicated low impurity levels of 1350 and 780 ppm for H and O, respectively.

XRD and electron diffraction patterns indicated that all of the Ni-W foils were single-phase with an FCC structure, suggesting a solid solution alloy. Although the equilibrium phase diagram of the Ni-W system is speculative at room temperature, W is expected to dissolve in Ni up to ~12.5 at% [10]. The electrodeposited foils listed in Table II are noted to be very close to this limit. Grain sizes of the Ni-W foils were determined either directly from HREM images, or indirectly, from the XRD data. The results, included in Table II, are found to be well clustered in the range below 10 nm.

The structure of the Ni-W alloy deposited at a current density of 0.10 A/cm^2, which exhibits the main features of all of the specimens investigated, is shown in Fig. 1. The grain shape is apparently isotropic, and there is no obvious tendency for grains with a similar orientation to cluster together. Presumably, grain boundaries are mostly of the high-angle variety.

Fig. 1 Bright field image of nanocrystalline Ni-W alloy deposited at a current density of 0.10 A/cm^2.

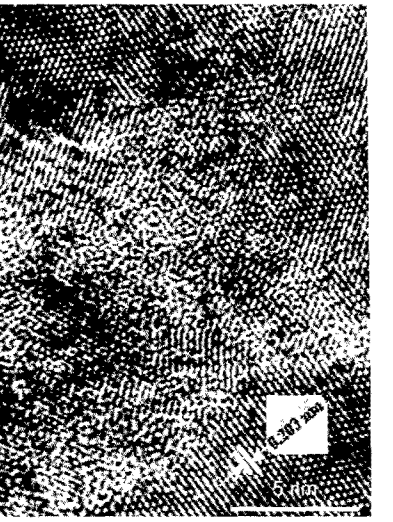

Fig. 2 A high-resolution image of the same Ni-W foil from Fig. 1.

A high-resolution image of Fig. 1 showing the detailed structure of the Ni-W foil is presented in Fig. 2. This figure is filled with fine domains of lattice fringes with a spacing of 0.203 nm, which is the spacing of the {111} plane of Ni. The grain size is estimated to be about 4.5-6.2 nm, and the intercrystalline regions (i.e., grain boundaries and triple junctions) are manifested as structureless bands about 0.5-1 nm wide. The images also indicate that the grains are approximately equiaxed, with no notable morphological anisotropy.

The effect of applied current density on the nanostructure of the Ni-W alloys is illustrated in Figs. 3 and 4, which are planar views of the specimens deposited at (a) 0.05 and (b) 0.15 A/cm^2, respectively. These figures can be directly compared with Fig. 2, which is the corresponding image from sample produced with an intermediate current density of 0.10 A/cm^2. Although the current density has little effect on the grain size and the global concentration of W in the alloys (Table II), these figures show that current density greatly affect the texture of the deposited films, and generally a higher current density results in a more random orientation (Fig. 4).

Existence of structureless region

As discussed in Fig. 2, grain boundaries and triple junctions exhibit as structureless bands (or amorphous bands). High-resolution images taken from Figure 1 show that, in fact, there are two types of grain boundary. One type of grain boundary is a high-angle boundary but does not exhibit a band structure (marked by arrows in Fig. 5a), i.e. crystal lattices of neighboring grains have an intimate contact. Another type is the grain boundary exhibiting as a structureless band surrounding a grain (marked in Fig. 5b), i.e. the crystal lattices of neighboring grains are separated by structureless bands. The former is a typical grain boundary for nanocrystalline pure Ni produced by electrodeposition, while the latter is for alloyed Ni.

Prior research has shown that Ni-W alloys can be refined to a fully amorphous structure [8]. A corresponding dark field image of Fig. 1 is shown in Fig. 6. Grain size is estimated to be

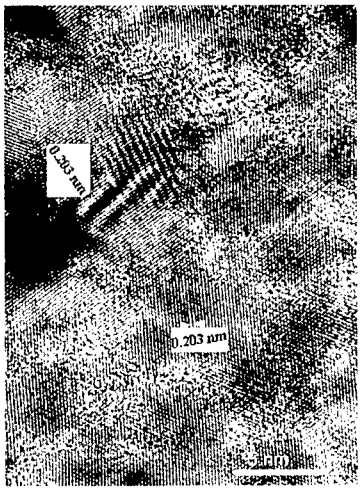

Fig. 3 High-resolution image of nanocrystalline Ni-W alloys deposited at a current of 0.05 A/cm^2.

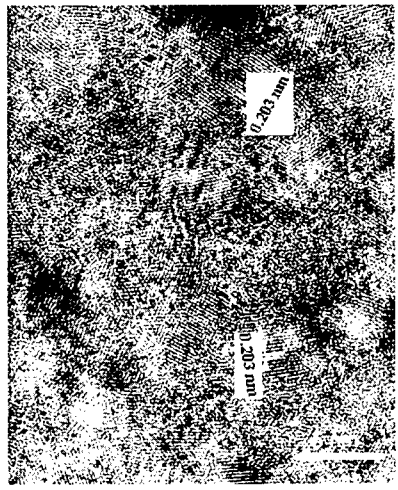

Fig. 4 High-resolution mage of nanocrystalline Ni-W alloy deposited at a current of 0.15 A/cm^2.

Fig. 5 High-resolution image of nanocrystalline Ni-W alloy deposited at a current density of 0.10 A/cm^2, showing high-angle boundaries without structureless layer (a) and grain boundaries with a structureless phase separating two neighboring grains (b).

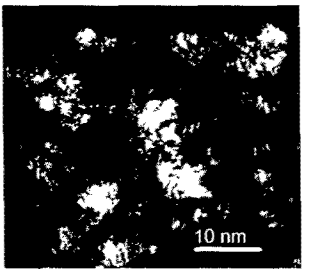

Fig. 6 Dark field image taken from the sample used for Fig. 1.

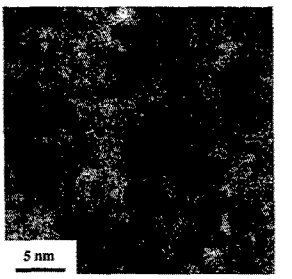

Fig. 7 STEM bright image of the sample used for Fig. 6.

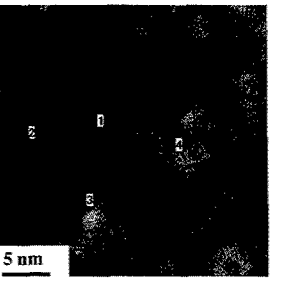

Fig. 8 HAADF image showing Z contrast caused by density difference.

about 5 nm. A close inspection of this figure shows the existence of many very small bright spots. These bright spots are structureless phase includes very short-range ordered crystals.

To further investigate the W distribution, a STEM image from the sample used for Fig. 1 is shown in Fig. 7. This figure does not show the lattice image because STEM observation is not available for taking the image. The angular dark field image (i.e. Z-contrast) of Fig. 7 is shown in Fig. 8. In Fig. 8, the dark field contrast that arises from the difference of local density in the material; specifically, a brighter spot indicates a higher density. Chemical analyses were subsequently carried out at a dark region (Point 1) and a bright region (Point 4) in Fig. 8, and the results are shown in Fig. 9. From the intensities at 1.774 keV for W and 7.471 keV for Ni, the atomic percents were calculated at Points 1 and 4. Tungsten contents were 8 at% and 14 at% at Points 1 and 4, respectively. It is noted that the tungsten content at Point 4 is over the equilibrium solubility limit of 12.5 at% at room temperature. Electrodeposition is, in principle, like rapid solidification process, which usually produces metastable phase or even amorphous phase. The structureless bands shown in Fig 5b is thereby proposed to be a metastable phase caused by the local supersaturation of W in Ni. Watanabe [14] recently reported that if the affinity between an alloying element and the matrix element is stronger than that between the same elements, the alloying system has high potential to produce an amorphous phase. His simulations showed that amorphous-like structure occurs in a binary system when the alloying content is about 20 at%. The mixed phase structure obtained in this study is in a transitional stage from nanocrystalline state to amorphous state.

CONCLUSIONS

Nanocrystalline Ni-W alloys were synthesized using an electrodeposition method, and their structure investigated. The main results of this work are:

1) The Ni-W alloys all have similar composition (~13 at% W) and grain size (d ~ 4-9 nm), and the texture of the foils varies depending on the deposition current density.

2) There are two types of grain boundaries in nanocrystalline Ni. One type of grain boundary is of one atomic layer thin and another type consists of a structureless layer of about 0.5-1 nm in thickness.

3) The formation of structureless phase is characteristic for the electrodeposited Ni-W alloys. The structureless band is probably a metastable phase caused by the local supersaturation of W in Ni.

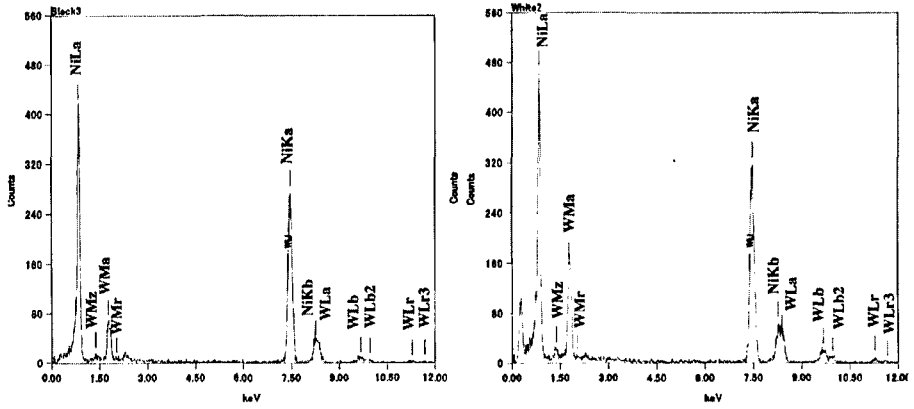

Fig. 9 Chemical analysis from Points 1 and 4 in Fig. 8. The W content at Point 4 is higher than that at Point 1.

REFERENCES

1. R.T.C. Choo, J.M. Toguri, A.M. El-Sharik, U.Erb, *Journal of Applied Electrochemistry* **25**, 384 (1995).
2. H. Natter, M. Schmelzer, R. J. Hempelmann, *Mater. Res.* **13**, 1186 (1998).
3. M.L. Trudeau, *Nanostructured Materials* **12,** 55 (1999).
4. D.L. Grimmett, M. Schwartz, K. Nobe, *Journal of the Electrochemical Society* **140,** 973 (1993).
5. U. Erb, *Nanostructured Materials* **6,** 533 (1995).
6. U. Erb, A.M. El-Sharik, G . Palumbo, K.T. Aust, *Nanostructured Materials* **2,** 383 (1993).
7. A. Inoue, *Acta Mater.* **48,** 279 (2000).
8. T. Yamasaki, R. Tomohira, Y. Ogino, P. Schlossmacher, K. Ehrlich, *Plating and Surface Finishing* **87,** 148 (1999).
9. T. Yamasaki, *Scripta Mater.* **44,** 1497 (2001).
10. *ASM Handbook: Alloy Phase Diagrams.* Vol. 3. 1992, Metals Park, OH: ASM.
11. T. Watanabe, *Materialia Japan* **40,** 871 (2001).